Electric Power Systems Research 214 (2023) 108798

Contents lists available at ScienceDirect

Electric Power Systems Research

journal homepage: www.elsevier.com/locate/epsr

Steady-state power distribution in VSC-based MTDC systems and dc grids under mixed P/V and I/V droop control

Pingyang Sun [a,*], Yingqi Wang [b], Muhammad Khalid [c], Ramon Blasco-Gimenez [d], Georgios Konstantinou [a]

[a] School of Electrical Engineering and Telecommunications, UNSW Sydney, Sydney, NSW, 2052, Australia
[b] School of Electrical and Data Engineering, University of Technology Sydney, NSW, 2007, Australia
[c] Electrical Engineering Department & Center for Renewable Energy and Power Systems, King Fahd University of Petroleum & Minerals, Dhahran, 31261, Saudi Arabia
[d] Department of Systems Engineering and Control, Technical University of Valencia, Valencia, 46022, Spain

ARTICLE INFO

Keywords:
Power distribution
Voltage source converter (VSC)
Multi-terminal HVDC (MTDC) systems
Dc grids
Mixed P/V and I/V droop control

ABSTRACT

This paper proposes a steady-state power distribution derivation method for voltage source converter (VSC)-based multi-terminal HVDC (MTDC) systems and dc grids under mixed power/voltage (P/V) and current/voltage (I/V) droop control. P/V and I/V droop control are two commonly used control schemes, which can be combined to achieve co-regulation of powers & currents in MTDC systems and dc grids. The proposed method can be used to estimate the power distributions under different scenarios for MTDC systems and dc grids based on VSCs with mixed P/V and I/V droop control. After determining the initial operating point based on an estimation-correction algorithm, redistributed power due to power disturbances, current changes or converter outages is analyzed in detail considering converter overload. An excess power reduction strategy is further proposed to avoid violation of power limits after converter outage. The accuracy of the proposed method is validated through multiple scenarios in a modular multilevel converter (MMC)-based four-terminal dc grid. The comparison between the proposed method and other approaches in the current literature further demonstrates the advantages of proposed power distribution derivation method.

1. Introduction

High-voltage direct current (HVDC) transmission has become an irreplaceable part of many modern electricity grids due to its unique benefits [1]. Voltage source converters (VSCs) offer flexible power reversal capability and provide immunity to commutation failures compared to conventional line-commutated converters (LCCs). Therefore, VSCs are more suitable for multiterminal HVDC (MTDC) systems and future dc grids. Moreover, modular VSCs as typical modular multilevel converter (MMC) show improved performance than two-level or three-level VSCs due to modularity and scalability [2–4]. Many MMC-based MTDC projects are commissioned and under construction in the world, such as Zhoushan [5] five-terminal HVDC system and Zhangbei [6] four-terminal dc grid.

The basic system level control schemes for VSC-based MTDC systems and dc grids can be categorized into (*i*) master–slave control [7], (*ii*) dc voltage margin control [8] and (*iii*) droop control [9–18]. In the first two control schemes, one converter is arranged to control the dc voltage of the whole HVDC system. However, the whole system would be out of control after the outage of the converter tasked with constant dc voltage control. On the other hand, two or more converters coordinate to balance the dc voltage via fixed [9] or variable [11] droop constants in droop control, hence the system reliability can be improved.

Power or current sharing [9,12] and frequency support [14] can be achieved in different droop control schemes. The values of fixed droop constants are based on the power ratings of all converters in an MTDC system and a dc grid [9]. The use of variable droop constants avoids converter overloading after large power disturbances at the cost of complex controller design [11]. Power/voltage (P/V) droop is a typical droop control scheme in VSC-based dc systems, and the objective of power control can be ac active power or dc power depending on actual requirements [9]. Current/voltage (I/V) droop is another droop control method where the control objective is regulation of dc current instead of power [13]. Also, frequency control can be used with both P/V or I/V droop control for providing frequency support of ac systems [14].

* Corresponding author.
E-mail address: pingyang.sun@student.unsw.edu.au (P. Sun).

https://doi.org/10.1016/j.epsr.2022.108798
Received 1 July 2022; Received in revised form 6 September 2022; Accepted 6 September 2022
Available online 18 September 2022

It is critical to conduct steady-state system performance analysis, which can assess static security of VSC-based MTDC systems and dc grids under different operating scenarios [10,19]. Updated power distribution can be derived after a change in either power or dc current Ref. [9,10,13]. In addition, power redistribution is also explored after converter outages under P/V or I/V droop control [10,13,15]. An analytical method allows derivation of power distribution under P/V droop control after converter outage, taking converter overloads into consideration [10].

P/V droop control can achieve power sharing and desired power in each converter that can be obtained directly according to pre-set droop constants. Moreover, the desired power can be obtained indirectly by determining the value of dc current under I/V droop control. Direct regulation of dc current is important in a VSC-based MTDC system or dc grid, since possible dc current interruption and over-current operation can be avoided by setting minimum/maximum current limits in the dc current control unit. Therefore, co-regulation of powers and currents can be achieved by combining P/V and I/V droop control schemes, making them attractive for MTDC systems and dc grids. Mixed P/V and I/V droop control is considered in [16,20,21] to study comprehensive power flow model and decoupled ac/dc power flow computation, respectively.

The detailed power distribution analysis for VSC-based MTDC systems and dc grids after system disturbances, including the reference change and converter outage, is not discussed in the current literature [9,10,13,15,16,20–22]. Although power redistribution after converter outage under mixed P/V and I/V droop control in an LCC and VSC-based dc grid has discussed in [22], the dc current direction has to be determined first leading to complicated calculation. In addition, two special scenarios are not discussed that all remaining converters located at rectifier and inverter side may violate power limits after converter outages. For obtaining the power distribution after different system disturbances, the initial operating point should be determined first. This initial operating point can be calculated by pre-defining different voltage, power and current nodes, which requires definition and solution of multiple jacobian matrices [20].

This paper proposes a power node-based estimation-correction algorithm to determine the initial operating point for mixed P/V and I/V droop control. The terminal dc powers with known dc currents are estimated first, then the accurate power values are obtained by iteration correction. It is noteworthy that only one general jacobian matrix needs to be established in the proposed algorithm. Moreover, the power redistribution after dc power/current reference change and converter outage are analyzed, while converter overload is considered for ensuring static security of a VSC-based MTDC system or dc grid. In order to avoid all remaining converters violate their power limits, the dc powers in rectifier or inverter side could be reduced and the detailed reduction strategy is analyzed. The accuracy of the proposed power distribution derivation method is verified in an MMC-based four-terminal dc grid by examining the consistency between theoretical derivation and simulation results.

There are three main contributions in this paper: (*i*) a power node-based initial operating point determination algorithm is proposed for avoiding defining multiple jacobian matrices under mixed P/V and I/V droop control [20]; (*ii*) the current power distribution analysis under single P/V droop control [9,10] is extended to be applied in mixed droop control, considering different system disturbances (dc power/current reference changes and converter outages); (*iii*) a detailed converter overload analysis under mixed droop control is also provided based on the analytical approach for P/V droop control in [10].

The paper is structured as follows. Section 2 provides a general description of VSC-based MTDC systems and dc grids including basic control hierarchy and static characteristic of droop control. The detailed steady-state system performance under mixed P/V and I/V droop control is described in Section 3, while Section 4 conducts theory derivation and simulation verification in a four-terminal MMC-based dc grid. Section 5 discusses the obtained power distribution results and compares the proposed power distribution derivation method with other approaches. Section 6 summarizes the conclusions of the article.

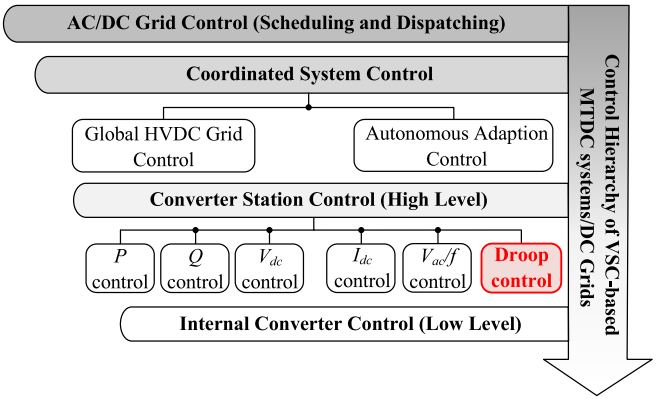

Fig. 1. Control hierarchy of VSC-based MTDC systems and dc grids.

2. VSC-based MTDC systems and DC grids

2.1. Control hierarchy

The basic control hierarchy of the VSC-based MTDC systems and dc grids consists of four main layers: (*i*) ac/dc grid control, (*ii*) coordinated system control, (*iii*) converter station control, and (*iv*) internal converter control (Fig. 1). The first layer is for necessary scheduling and dispatching of VSC-based MTDC systems and dc grids. The coordinated system control (second layer) defines the reference set-points for VSCs and handles unscheduled events [23].

Moreover, the third layer functions as converter station control to regulate ac active/reactive power, dc power, node voltages/currents, system frequency and specified droop control is also included in this layer. The bottom layer is the internal converter control for VSCs such as circulating current control [24,25], submodule (SM)-based control [26,27] and related internal control for different modular VSCs [28,29].

2.2. Static characteristic of droop control

The static characteristic and controller structure of droop control are shown in Fig. 2, where a three terminal HVDC system is adopted as an example. VSC1 (rectifier) delivers power to VSC2 and VSC3 (inverters), and dc voltage is balanced by all three converters via corresponding droop characteristic. Matrix $\boldsymbol{K_{droop}}$ represents the droop constants of all converters in an MTDC system or a dc grid, and the ratio of characteristic curve is defined as $\boldsymbol{R} = (\boldsymbol{K_{droop}})^{-1}$ [9,10].

When an MTDC system or a dc grid with droop control is in steady-state operation, (1) and (2) can be established for P/V droop control and I/V droop control, respectively.

$$(\boldsymbol{P_{dc}^{PV*}} - \boldsymbol{P_{dc}^{PV}}) + \mathrm{diag}(\boldsymbol{K_{droop}^{PV}})(\boldsymbol{V_{dc}^{PV*}} - \boldsymbol{V_{dc}^{PV}}) = \boldsymbol{0}, \tag{1}$$

$$(\boldsymbol{I_{dc}^{IV*}} - \boldsymbol{I_{dc}^{IV}}) + \mathrm{diag}(\boldsymbol{K_{droop}^{IV}})(\boldsymbol{V_{dc}^{IV*}} - \boldsymbol{V_{dc}^{IV}}) = \boldsymbol{0}, \tag{2}$$

where the superscript * refers to reference values. The droop constants for P/V and I/V droop control are defined as (3) and (4), respectively.

$$K_{droop}^{PV} = \frac{P_{dc,rated}}{V_{dc,rated}\delta_{droop}}\ (\mathrm{MW/kV}), \tag{3}$$

$$K_{droop}^{IV} = \frac{P_{dc,rated}}{V_{dc,rated}^2\delta_{droop}}\ (\mathrm{kA/kV}), \tag{4}$$

where $P_{dc,rated}$ and $V_{dc,rated}$ is the rated dc power and rated dc voltage of each converter, respectively, and δ_{droop} refers to the allowable dc voltage deviation ratio [9]. It is noted that the converter will run in constant dc power (dc current) control or dc voltage control if $K_{droop} = 0$ or $K_{droop} = \infty$, respectively.

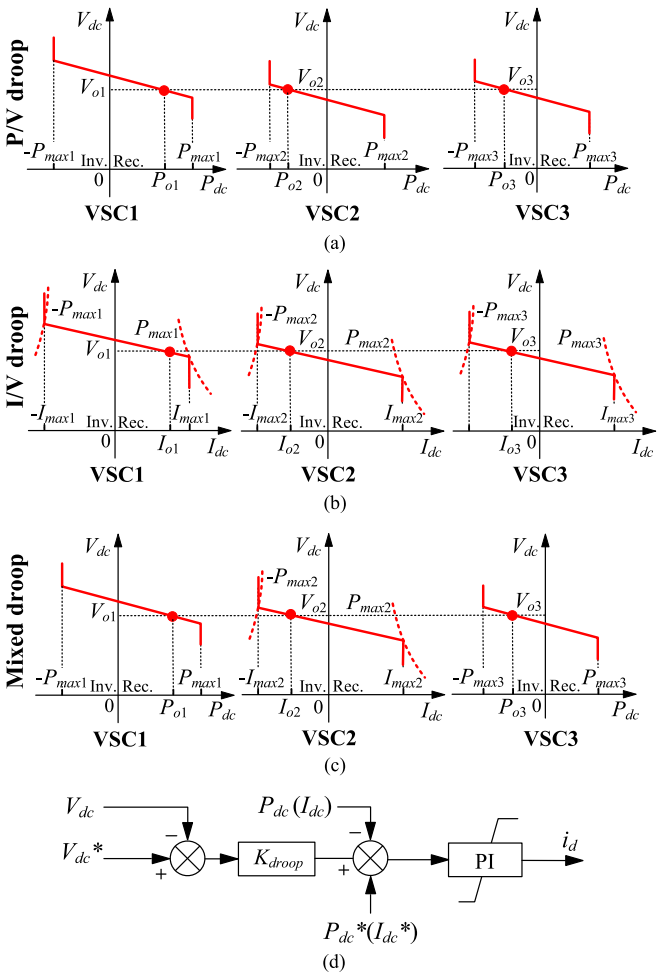

Fig. 2. Static characteristic of droop control in VSC-based MTDC systems and dc grids: (a) single P/V droop control, (b) single I/V droop control, (c) mixed P/V and I/V droop control, and (d) structure of droop controller.

3. Proposed power distribution derivation method under mixed P/V and I/V droop control

3.1. Initial operating point determination

For an MTDC system or a dc grid of n buses under P/V droop control, the initial steady-state condition is one known dc voltage and $n-1$ known dc powers. Without loss of generality, the first VSC is assumed to operate as dc slack bus. The initial power distribution can be solved by Newton–Raphson method, obtaining one dc power and $n-1$ dc voltages [9]. The dc power injected to dc buses with one known dc voltage and $n-1$ known dc powers can be expressed as:

$$\begin{cases} P^{PV}_{dc1,ini} = V^{PV}_{dc1,ini}\sum_{j=1}^{n} G_{dc_{1j}} V^{PV}_{dcj,ini}, \\ P^{PV}_{dci,ini} = V^{PV}_{dci,ini}\sum_{j=1}^{n} G_{dc_{ij}} V^{PV}_{dcj,ini} \quad (i=2,3,\dots,n), \end{cases} \tag{5}$$

where $V^{PV}_{dc1,ini}$ is dc bus voltage with known dc voltage, $V^{PV}_{dci,ini}$ is dc bus voltages with known dc powers, and $G_{dc_{ij}}$ is line conductance. Moreover, (6) can be obtained from (5).

$$\Delta P^{PV}_{dci,ini} = P^{PV}_{dci,ini} - V^{PV}_{dci,ini}\sum_{j=1}^{n} G_{dc_{ij}} V^{PV}_{dcj,ini} = 0 \quad (i=1,2,\dots,n). \tag{6}$$

Therefore, the relationship between $\boldsymbol{\Delta P^{PV}_{dc}}$ and $\boldsymbol{\Delta V^{PV}_{dc}}$ can be established as:

$$\boldsymbol{\Delta P^{PV}_{dc,ini}} = \boldsymbol{J^{PV}_{dc}}\,\boldsymbol{\Delta V^{PV}_{dc,ini}}, \tag{7}$$

where $\boldsymbol{J^{PV}_{dc}} = -\frac{\partial \Delta P^{PV}_{dc,ini}}{\partial V^{PV}_{dc,ini}} = \mathrm{diag}(\boldsymbol{V^{PV}_{dc,ini}})\boldsymbol{G_{dc}} + \mathrm{diag}(\boldsymbol{G_{dc}}\boldsymbol{V^{PV}_{dc,ini}})$.

However, the above calculation cannot determine the initial operating point for mixed P/V and I/V droop control, because the initial steady-state dc powers of certain VSCs with I/V droop control cannot be derived directly. In order to avoid the definition of multiple jacobian matrices [20], an estimation-correction algorithm is proposed in this paper by modifying (5) in single P/V droop control. In the case that converter m adopts I/V droop control and other converters adopt P/V droop control, the initial dc power for converter m is estimated as:

$$P^{IV,est}_{dcm,ini} = V_{dc,rated} I^{IV,targ}_{dcm,ini}, \tag{8}$$

where $I^{IV,targ}_{dcm,ini}$ is the pre-specified dc current value (initial steady-state condition) for certain VSC with I/V droop control. This is stage 1 (power estimation) in the proposed algorithm. In the following stage (stage 2), correction iterations are conducted since there is a dc power deviation ($\Delta P^{IV,cor}_{dcm,ini}$) between the estimated and actual dc power m. Hence, the actual initial dc power for a VSC with I/V droop control can be expressed as:

$$P^{IV,act}_{dcm,ini} = P^{IV,est}_{dcm,ini} + \Delta P^{IV,cor}_{dcm,ini}. \tag{9}$$

In the correction iteration process, the iteration step size and range should be decided. The step size depends on the calculation precision (e.g. 10^{-1} for 1 decimal place). Moreover, the iteration range can be obtained by the maximum allowable power deviation for the terminal m with initial dc current, which is determined by the dc voltage deviation δ_{droop}, thus the maximum range is from $-V_{dc,rated}\delta_{droop} I^{IV,targ}_{dcm,ini}$ to $V_{dc,rated}\delta_{droop} I^{IV,targ}_{dcm,ini}$.

The accurate initial dc power for certain I/V droop-based VSC with known initial dc current can be obtained by setting the initial steady-state dc current as iteration target. If the deviation between the target and obtained dc currents is very small (10), the corresponding dc powers in (5) will be substituted by the corrected powers as expressed in (11). Following the algorithm flowchart in the red box of Fig. 3, the initial operating point is determined for mixed P/V and I/V droop-controlled VSC MTDC systems or dc grids.

$$\left| I^{IV,targ}_{dcm,ini} - \frac{P^{IV,act}_{dcm,ini}}{V^{IV}_{dcm,ini}} \right| < \text{error} \tag{10}$$

$$\begin{bmatrix} P^{PV}_{dc1,ini} \\ \vdots \\ V_{dcr} I^{IV}_{dcm,ini} + \Delta P^{IV}_{dcm,ini} \\ \vdots \\ P^{PV}_{dcn,ini} \end{bmatrix} = \begin{bmatrix} V^{PV}_{dc1,ini} & & & & \\ & \ddots & & & \\ & & V^{IV}_{dcm,ini} & & \\ & & & \ddots & \\ & & & & V^{PV}_{dcn,ini} \end{bmatrix} \times \begin{bmatrix} G_{dc11} & G_{dc12} & G_{dc13} & \cdots & G_{dc1n} \\ G_{dc21} & G_{dc22} & G_{dc23} & \cdots & G_{dc2n} \\ G_{dc31} & G_{dc32} & G_{dc33} & \cdots & G_{dc2n} \\ \vdots & \vdots & \vdots & \ddots & \vdots \\ G_{dcn1} & G_{dcn2} & G_{dcn3} & \cdots & G_{dcnn} \end{bmatrix} \begin{bmatrix} V^{PV}_{dc1,ini} \\ \vdots \\ V^{IV}_{dcm,ini} \\ \vdots \\ V^{PV}_{dcn,ini} \end{bmatrix} \tag{11}$$

3.2. Power distribution after reference change

The dc powers, currents, voltages in a VSC-based MTDC system or dc grid vary with the change of reference values ($\boldsymbol{\Delta P^{*}_{dc}}, \boldsymbol{\Delta I^{*}_{dc}}, \boldsymbol{\Delta V^{*}_{dc}}$). Considering P/V and I/V droop control and assuming $\boldsymbol{\Delta x} = \boldsymbol{x} - \boldsymbol{x_{ini}}$ ($\boldsymbol{x}$ represents column vectors of different variables), (1) and (2) can be further expressed as (12) and (13), respectively.

$$\boldsymbol{\Delta P^{PV}_{dc}} - \boldsymbol{\Delta P^{PV*}_{dc}} = \mathrm{diag}(\boldsymbol{K^{PV}_{droop}})(\boldsymbol{\Delta V^{PV*}_{dc}} - \boldsymbol{\Delta V^{PV}_{dc}}) \tag{12}$$

$$\Delta \boldsymbol{I}_{dc}^{IV} - \Delta \boldsymbol{I}_{dc}^{IV*} = \mathrm{diag}(\boldsymbol{K}_{droop}^{IV})(\Delta \boldsymbol{V}_{dc}^{IV*} - \Delta \boldsymbol{V}_{dc}^{IV}) \tag{13}$$

In addition, the relationship between $\Delta \boldsymbol{P}_{dc}$ and $\Delta \boldsymbol{V}_{dc}$ can be obtained in the initial operating point determination as:

$$\Delta \boldsymbol{P}_{dc} = \boldsymbol{J}_{dc} \Delta \boldsymbol{V}_{dc}, \tag{14}$$

where $\boldsymbol{J}_{dc}$ is dc jacobian matrix of a given MTDC system or dc grid under mixed P/V and I/V droop control. Moreover, the relationship between $\Delta \boldsymbol{I}_{dc}$ and $\Delta \boldsymbol{V}_{dc}$ is:

$$\Delta \boldsymbol{I}_{dc} = \boldsymbol{G}_{dc} \Delta \boldsymbol{V}_{dc}. \tag{15}$$

Furthermore, (16) can be derived by combining (14) and (15).

$$\Delta \boldsymbol{I}_{dc} = \boldsymbol{G}_{dc} \boldsymbol{J}_{dc}^{-1} \Delta \boldsymbol{P}_{dc} = \boldsymbol{M}_{dc} \Delta \boldsymbol{P}_{dc}, \tag{16}$$

which is used to replace ΔI_{dcm}^{IV} with ΔP_{dcm}^{IV} in following calculations. Supposing no change of dc voltage references ($\Delta \boldsymbol{V}_{dc}^{*} = \boldsymbol{0}$), $\Delta \boldsymbol{V}_{dc}$ in (14) can be re-expressed as (17) by reconstructing (12) and (13).

$$\begin{cases} \Delta \boldsymbol{V}_{dc}^{PV} = \mathrm{diag}(\boldsymbol{K}_{droop}^{PV})^{-1}(\Delta \boldsymbol{P}_{dc}^{PV*} - \Delta \boldsymbol{P}_{dc}^{PV}) \\ \Delta \boldsymbol{V}_{dc}^{IV} = \mathrm{diag}(\boldsymbol{K}_{droop}^{IV})^{-1}(\Delta \boldsymbol{I}_{dc}^{IV*} - \Delta \boldsymbol{I}_{dc}^{IV}) \end{cases} \tag{17}$$

Therefore, (18) can be derived by substituting (17) into (14), and dc current deviation for converter m with I/V droop control in (18) is calculated as:

$$\begin{bmatrix} K_{droop1}^{PV} & & & & \\ & \ddots & & & \\ & & K_{droopm}^{IV} & & \\ & & & \ddots & \\ & & & & K_{droopn}^{PV} \end{bmatrix} \times \begin{bmatrix} J_{dc11} & J_{dc12} & J_{dc13} & \cdots & J_{dc1n} \\ J_{dc21} & J_{dc22} & J_{dc23} & \cdots & J_{dc2n} \\ J_{dc31} & J_{dc32} & J_{dc33} & \cdots & J_{dc2n} \\ \vdots & \vdots & \vdots & \ddots & \vdots \\ J_{dcn1} & J_{dcn2} & J_{dcn3} & \cdots & J_{dcnn} \end{bmatrix}^{-1} \times \begin{bmatrix} \Delta P_{dc1}^{PV} \\ \vdots \\ \Delta P_{dcm}^{IV} \\ \vdots \\ \Delta P_{dcn}^{PV} \end{bmatrix} = \begin{bmatrix} \Delta P_{dc1}^{PV*} - \Delta P_{dc1}^{PV} \\ \vdots \\ \Delta I_{dcm}^{IV*} - \Delta I_{dcm}^{IV} \\ \vdots \\ \Delta P_{dcn}^{PV*} - \Delta P_{dcn}^{PV} \end{bmatrix} \tag{18}$$

$$\Delta I_{dcm}^{IV} = M_{m1} \Delta P_{dc1}^{PV} + \cdots + M_{mm} \Delta P_{dcm}^{IV} + \cdots + M_{mn} \Delta P_{dcn}^{PV} \tag{19}$$

The dc power variations can be obtained by combining (18) and (19) if there are no overloaded converters. Also, the dc voltage deviations are further derived by $\Delta \boldsymbol{V}_{dc} = \boldsymbol{J}_{dc}^{-1} \Delta \boldsymbol{P}_{dc}$.

If one VSC is overloaded as (20) after preliminary calculation, the converter should be in constant dc power or current control in actual operation. The actual dc power or current variation of such a converter with P/V or I/V droop control can be calculated as (21) and (22), respectively.

$$\left| P_{dci,ini} + \Delta P_{dci}^{pre} \right| > P_{dci,rated} \tag{20}$$

$$\Delta P_{dci}^{PV,act} = P_{dci}^{PV,max} - P_{dci,ini}^{PV} \tag{21}$$

$$\begin{cases} \Delta I_{dcl}^{IV,act} = M_{l1} \Delta P_{dc1} + \cdots + M_{ll} \Delta P_{dcl}^{IV,act} + \cdots + M_{ln} \Delta P_{dcn} \\ \Delta P_{dcl}^{IV,act} = P_{dcl}^{IV,max} - P_{dcl,ini}^{IV} \end{cases} \tag{22}$$

Moreover, the droop constants for overloaded converters should be set to zero as:

$$\begin{cases} K_{droopi}^{PV} = 0 \\ K_{droopl}^{IV} = 0 \end{cases} \tag{23}$$

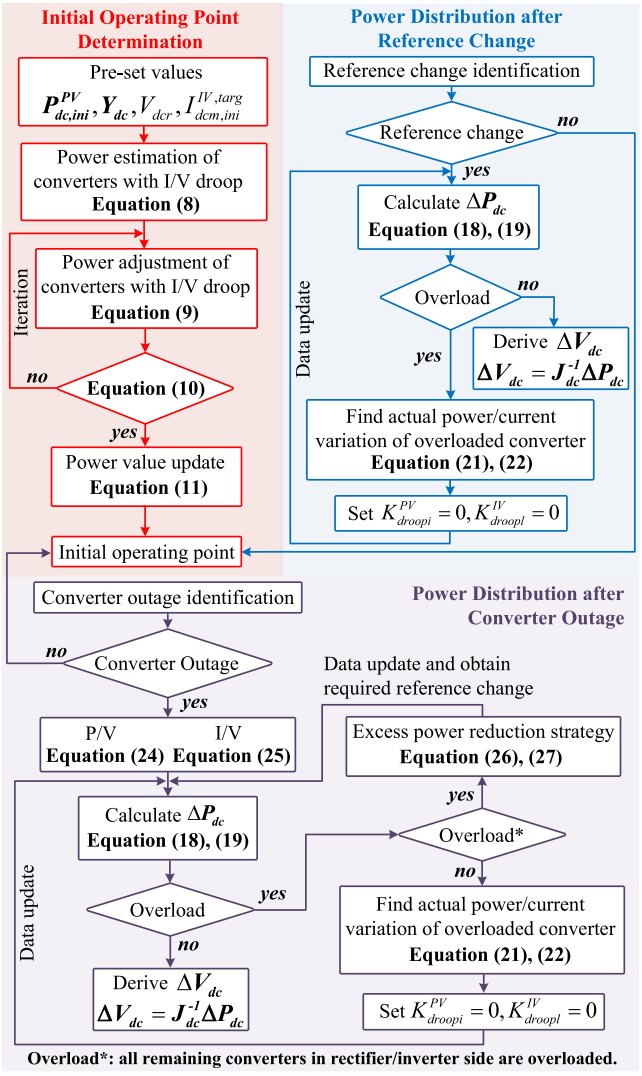

Fig. 3. Flowchart of proposed power distribution derivation method under mixed P/V and I/V droop control.

The dc power variations can be accurately derived by substituting (21), (22) and (23) into (18), hence obtaining the final power distribution after reference change considering converter power limitation. The whole calculation flowchart is shown in the blue box of Fig. 3.

3.3. Power distribution after converter outage & Excess power reduction strategy

Different from the power distribution analysis after reference change, the outage of a certain converter under P/V or I/V droop control in an MTDC system or a dc grid can be summarized as:

$$\begin{cases} \Delta P_{dck}^{PV*} = -P_{dck,ini}^{PV}, \\ K_{droopk}^{PV} = 0, \end{cases} \tag{24}$$

or

$$\begin{cases} \Delta I_{dcj}^{IV*} = -I_{dcj,ini}^{IV}, \\ K_{droopj}^{IV} = 0. \end{cases} \tag{25}$$

Substituting (24) and (25) into (18) and (19), $\Delta \boldsymbol{P}$ can be derived and the power distribution will be further obtained if all VSCs do not hit power limitations.

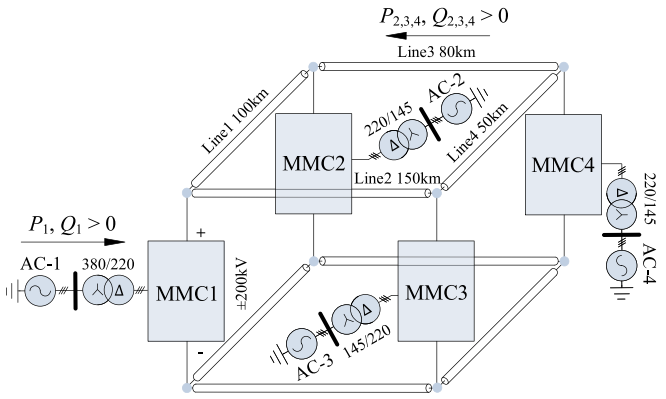

Fig. 4. MMC-based four terminal dc grid.

Table 1
Parameters of four MMCs in the dc grid.

Parameters	MMC1	MMC2	MMC3	MMC4
Rated power (MW)	800	400	150	250
DC voltage (kV)	±200	±200	±200	±200
AC voltage (kV)	380	145	145	145
Transformer ratio	380/220	145/220	145/220	145/220
Number of SMs per arm	400	400	400	400
Operating point (m_a)	0.9	0.9	0.9	0.9

It is also necessary to consider the power limits of VSCs after converter outages. The basic solution procedure is similar to the previous scenario of converter overloads after reference change. However, another condition should be further considered that the remaining VSCs in the rectifier or inverter side all reach power limits after converter outage. Therefore, an excess power reduction strategy is further proposed to decrease the total received or delivered power of each converter. The decreased value is equal to the sum of initial power values of isolated converters due to outages. In addition, the reduced power is distributed to each terminal based on each converter power rating. Thus, the column vectors of actual power variations in rectifier and inverter terminals can be expressed as:

$$\Delta \boldsymbol{P}_{\boldsymbol{dc}}^{\boldsymbol{rec}} = \frac{\sum P_{dc,ini}^{inv,outage}}{\sum P_{dc,rated}^{rec}} \boldsymbol{P}_{\boldsymbol{dc,rated}}^{\boldsymbol{rec}}, \quad \text{and} \tag{26}$$

$$\Delta \boldsymbol{P}_{\boldsymbol{dc}}^{\boldsymbol{inv}} = \frac{\sum P_{dc,ini}^{rec,outage}}{\sum P_{dc,rated}^{inv}} \boldsymbol{P}_{\boldsymbol{dc,rated}}^{\boldsymbol{inv}}, \tag{27}$$

respectively. Substituting (26) or (27) into (18) and (19), the required reference changes ($\Delta \boldsymbol{P}_{\boldsymbol{dc}}^{\boldsymbol{rec*}}$, $\Delta \boldsymbol{P}_{\boldsymbol{dc}}^{\boldsymbol{inv*}}$, $\Delta \boldsymbol{I}_{\boldsymbol{dc}}^{\boldsymbol{rec*}}$, $\Delta \boldsymbol{I}_{\boldsymbol{dc}}^{\boldsymbol{inv*}}$) can be determined as well. The detailed power redistribution solving flowchart after converter outage is described in the purple box of Fig. 3.

4. Case study and simulation verification

A detailed equivalent model of MMC-based four-terminal dc grid derived from the B4-57 DCS2 model [30] (Fig. 4) is built for verifying the accuracy of proposed power distribution under mixed P/V and I/V droop control. The parameters of four MMCs are listed in Tables 1, and 2 provides the parameters of dc transmission lines.

Three different control configurations (C1, C2 and C3) are used in the MMC-based dc grid. C1 is arranged to verify power distribution after reference change and converter outage with no overloads of all inverter or rectifier terminals. The purpose of arranging C2 and C3 aims to validate the feasibility of proposed excess power reduction strategy under overloads of all remaining inverter/rectifier terminals. In C1 and C2, MMC1 is located at rectifier side delivering power to MMCs 2–4, while MMC1 in the inverter side absorbs the power delivered from the other MMCs under C3. MMC2 adopts I/V droop control and MMC3 & MMC4 are with P/V droop control in the three control configurations. In addition, P/V droop control and constant dc power control are used in MMC1 under C1 and C2 & C3, respectively.

Table 2
Parameters of DC transmission lines in the MMC-based DC grid.

Parameters	Line 1	Line 2	Line 3	Line 4
Type	Cable	Cable	Cable	Cable
Distance (km)	100	150	80	50
Resistance (Ω/km)	0.011	0.011	0.011	0.011
Capacitance (μF/km)	0.2185	0.2185	0.2185	0.2185
Inductance (mH/km)	0.2615	0.2615	0.2615	0.2615
Maximum current (kA)	1.962			

Table 3
Pre-specified steady-state condition in the MMC-based dc grid.

Parameter		MMC1	MMC2	MMC3	MMC4
P_{dc} (MW)	C1, C2	–	–	−100	−120
	C3	–	–	100	120
I_{dc} (kA)	C1, C2	–	−0.95	–	–
	C3	–	0.95	–	–
V_{dc} (kV)	C1, C2	400	–	–	–
	C3	400	–	–	–
δ_{droop}		0.05	0.05	0.05	0.05
K_{droop}		40 MW/kV[a]	50 A/kV	7.5 MW/kV	12.5 MW/kV

[a]Droop constant of MMC1 is zero ($K_{droop1} = 0$) in C2 and C3.

Table 4
Initial operating point in the MMC-based dc grid under C1 and C2.

Parameter		MMC1	MMC2	MMC3	MMC4
P_{dc} (MW)	Calc.	601.0913	−377.9981	−100.0000	−120.0000
	Simu.	601.0913	−377.9981	−99.9999	−120.0000
V_{dc} (kV)	Calc.	400.0000	397.8927	398.2020	397.8788
	Simu.	400.0002	397.8927	398.2020	397.8788

Table 3 lists the pre-specified steady-state condition and droop constants of all MMCs for determining the initial operating point. The first stage is to estimate the dc power of MMC2 by known dc current and rated dc voltage ($I_{dc2,ini}^{IV,targ} = -0.95$ kA for C1 & C2, $I_{dc2,ini}^{IV,targ} = 0.95$ kA for C3, $V_{dcr} = 400$ kV). The estimated dc power is $P_{dc2,ini}^{IV,est} = -0.95\times400 = -380$ MW for C1 & C2 and $P_{dc2,ini}^{IV,est} = 0.95 \times 400 = 380$ MW for C3. Hence, the actual dc power of MMC2 is corrected as $P_{dc2,ini}^{IV,act} = (-380 + \Delta P_{dc2,ini}^{IV,cor})$ MW for C1 & C2 and $P_{dc2,ini}^{IV,act} = (380 + \Delta P_{dc2,ini}^{IV,cor})$ MW for C3 in stage 2. If $\left| I_{dc2,ini}^{IV,targ} - \frac{P_{dc2,ini}^{IV,act}}{V_{dc2,ini}^{IV}} \right| < 10^{-5}$, the dc power deviation can be obtained ($\Delta P_{dc2,ini}^{IV,cor} = 2.0019$ MW for C1 & C2, $\Delta P_{dc2,ini}^{IV,cor} = 1.9966$ MW for C3) and the corrected dc power of MMC2 is −377.9981 MW for C1 & C2 and 381.9966 MW for C3. Furthermore, the initial operating point is determined by replacing the values of two known dc powers, one corrected dc power and one known dc voltage into (11) shown in Tables 4 and 5. The nodal admittance matrix of this dc grid is:

$$\boldsymbol{G}_{\boldsymbol{dc}} = \begin{bmatrix} 0.7576 & -0.4545 & -0.3030 & 0 \\ -0.4545 & 1.0227 & 0 & -0.5682 \\ -0.3030 & 0 & 1.2121 & -0.9091 \\ 0 & -0.5682 & -0.9091 & 1.4773 \end{bmatrix} \tag{28}$$

Tables 4 and 5 also show the simulation results of initial operating point, which verifies the accuracy of proposed initial operating point determination algorithm.

Table 5
Initial operating point in the MMC-based dc grid under C3.

Parameter		MMC1	MMC2	MMC3	MMC4
P_{dc} (MW)	Calc.	−598.9249	381.9966	100.0000	120.0000
	Simu.	−598.9249	381.9964	100.0000	120.0000
V_{dc} (kV)	Calc.	400.0000	402.1017	401.7886	402.1110
	Simu.	400.0000	402.1017	401.7887	402.1110

4.1. Case 1: Power distribution after reference change under C1

This section considers power distribution in the dc grid after dc power reference change at MMC4 and dc current reference change at MMC2 under the first control configuration (C1). The possibility of converter overloads is also considered and related simulation results are used to compare with the calculation results.

4.1.1. Case 1.1: DC power reference change of MMC4

Fig. 5 shows the calculation results of dc power and voltage variations of four MMCs after dc power reference change of MMC4. Also, the solid lines represent the scenarios with converter overloads consideration, while data in dash lines are derived without considering the power limits of four MMCs. The dc power reference of MMC4 changes from −100 MW to 100 MW with a step size of 20 MW, while four critical points are specifically marked in Fig. 5 that MMC2 just reaches to the power limit when $\Delta P^{*}_{dc4} = 83.8023$ MW.

The power distribution after a 100 MW power disturbance in MMC4 ($\Delta P^{*}_{dc4} = 100$ MW) is studied in detail with simulation results. Following the calculation flowchart in the blue box of Fig. 3, the preliminary power variation of MMC2 is $\Delta P^{pre}_{dc2} = -26.2545$ MW, which shows MMC2 is overloaded ($|-377.9981 - 26.2545|$ MW > 400 MW). Thus, the maximum achievable power variation of MMC2 is $\Delta P^{IV,act}_{dc2} = -20.0019$ MW. The actual current variation of MMC2 is $\Delta I^{IV,act}_{dc2} = -0.0521$ kA by setting the droop constant of MMC2 to zero ($K^{IV}_{droop2} = 0$). The jacobian matrix of the MMC-based dc grid under C1 is:

$$\boldsymbol{J}^{\boldsymbol{C1}}_{\boldsymbol{dc}} = \begin{bmatrix} 304.5330 & -181.8182 & -121.2121 & 0 \\ -180.8603 & 405.9857 & 0 & -226.0754 \\ -120.6673 & 0 & 482.4179 & -362.0018 \\ 0 & -226.0675 & -361.7080 & 587.4740 \end{bmatrix}, \tag{29}$$

hence

$$\boldsymbol{M}^{\boldsymbol{C1}}_{\boldsymbol{dc}} = \begin{bmatrix} 0.2429 & 0.2430 & 0.2426 & 0.2430 \\ -0.1536 & -0.1527 & -0.1550 & -0.1552 \\ -0.0405 & -0.0410 & -0.0384 & -0.0410 \\ -0.0488 & -0.0493 & -0.0492 & -0.0468 \end{bmatrix}, \tag{30}$$

and $\boldsymbol{J}^{\boldsymbol{C1}}_{\boldsymbol{dc}} = \boldsymbol{J}^{\boldsymbol{C2}}_{\boldsymbol{dc}}$, $\boldsymbol{M}^{\boldsymbol{C1}}_{\boldsymbol{dc}} = \boldsymbol{M}^{\boldsymbol{C2}}_{\boldsymbol{dc}}$. The power variations and voltage deviations after a 100 MW power disturbance are calculated as:

$$\begin{cases} \boldsymbol{\Delta P}_{\boldsymbol{dc}} = [-48.5555, -22.0019, -10.7670, 80.7718]^T \text{ MW}, \\ \boldsymbol{\Delta V}_{\boldsymbol{dc}} = [1.2139, 1.3432, 1.4356, 1.5383]^T \text{ kV}. \end{cases} \tag{31}$$

Fig. 6 shows the waveforms of dc powers and voltages before/after power disturbance ($\Delta P^{*}_{dc4} = 100$ MW) in simulation. At 1.5 s, the dc power reference of MMC4 is gradually changed from −120 MW to −20 MW. The terminal dc voltages are increased due to the power reduction in the inverter side. The power reduction of MMC4 also leads to the power decrease in MMC1 and increase in MMC2/MMC3, respectively. The detailed steady-state voltage and power values are determined by droop characteristics of all four MMCs. Table 6 lists the corresponding calculation and simulation results of power distribution.

4.1.2. Case 1.2: DC current reference change of MMC2

Fig. 7 shows the calculation results of power variations and voltage deviations after dc current reference change of MMC2 from −0.2 kA to 0.2 kA with a 0.05 kA step size. It is noted that the dc current

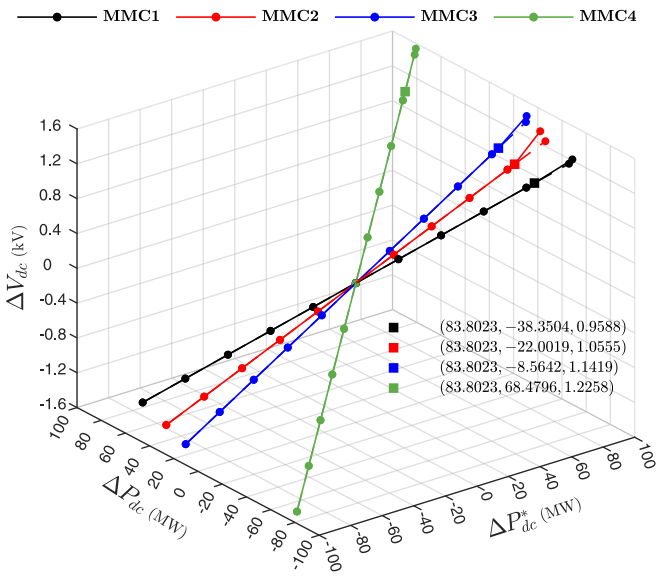

Fig. 5. Power variations and voltage deviations after dc power reference change of MMC4 from −100 MW to 100 MW.

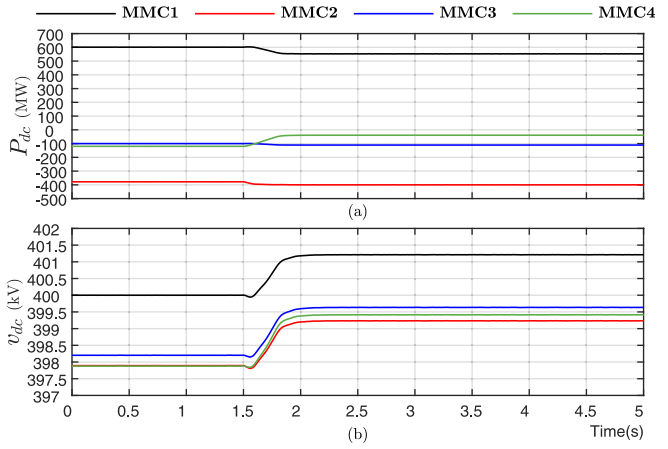

Fig. 6. Waveforms of dc powers and voltages after a 100 MW dc power reference change of MMC4 under C1: (a) DC powers and (b) dc voltages.

reference change of MMC2 may lead to overload of MMC2 itself. Four critical points are marked in Fig. 7 which indicate the minimum current reference change of MMC2 is −0.0780 kA and the maximum power variation of MMC2 is −20.0019 MW. The actual power variations and voltage deviations are represented with solid lines.

Table 7 lists power distribution calculation and simulation results when the current variation in MMC2 is less than −0.0780 kA ($\Delta I^{*}_{dc2} < -0.0780$ kA). By setting the droop constant of MMC2 to zero, the actual current variation of MMC2 can be derived ($\Delta I^{IV,act}_{dc2} = -0.0563$ kA). The obtained power variations and voltage deviations are:

$$\begin{cases} \boldsymbol{\Delta P}_{\boldsymbol{dc}} = [14.4476, -22.0019, 2.8324, 4.8838]^T \text{ MW}, \\ \boldsymbol{\Delta V}_{\boldsymbol{dc}} = [-0.3612, -0.4327, -0.3777, -0.3907]^T \text{ kV}. \end{cases} \tag{32}$$

In addition, the dynamic performance of dc powers and voltages after dc current reference change less than −0.0780 kA of MMC2 is shown in Fig. 8. In such case, the dc power in MMC2 (inverter side) is increased, resulting in the rise of system voltage. Therefore, MMC1 with droop control in the rectifier side delivers more power to remaining three MMCs. Moreover, the dc powers of MMC2 and MMC3 are decreased following individual droop characteristic curve.

Table 6
Power redistribution after dc power reference change of MMC4 under C1 (ΔP^*_{dc4} = 100 MW).

Parameter		MMC1	MMC2	MMC3	MMC4
P_{dc} (MW)	Calc.	552.5357	−400.0000	−110.7670	−39.2282
	Simu.	552.5596	−400.0000	−110.7566	−39.2071
V_{dc} (kV)	Calc.	401.2139	399.2359	399.6376	399.4171
	Simu.	401.2133	399.2348	399.6362	399.4154
K_{droop}		40 MW/kV	0	7.5 MW/kV	12.5 MW/kV

Table 7
Power redistribution after dc current reference change of MMC2 under C1 (ΔI^*_{dc2} < −0.0780 kA).

Parameter		MMC1	MMC2	MMC3	MMC4
P_{dc} (MW)	Calc.	615.5388	−400.0000	−97.1676	−115.1162
	Simu.	615.5413	−400.0000	−97.1667	−115.1157
V_{dc} (kV)	Calc.	399.6388	397.4600	397.8243	397.4881
	Simu.	399.6388	397.4599	397.8242	397.4881
K_{droop}		40 MW/kV	0	7.5 MW/kV	12.5 MW/kV

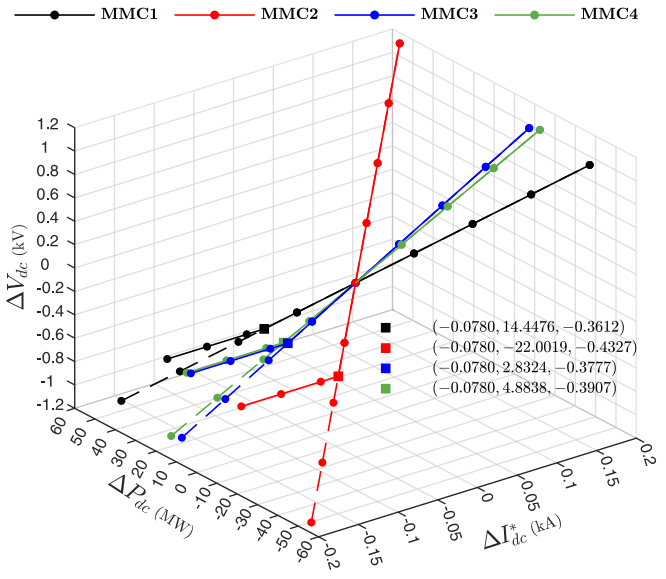

Fig. 7. Power variations and voltage deviations after dc current reference change of MMC2 from −0.2 kA to 0.2 kA.

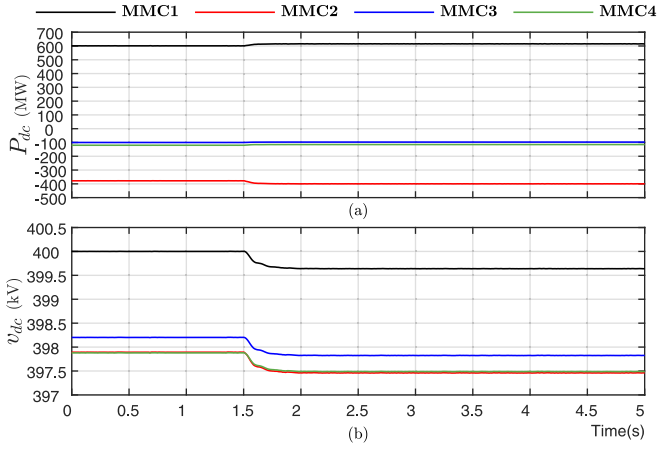

Fig. 8. Waveforms of dc powers and voltages after dc current reference change less than −0.0780 kA of MMC2 under C1: (a) DC power and (b) dc voltage.

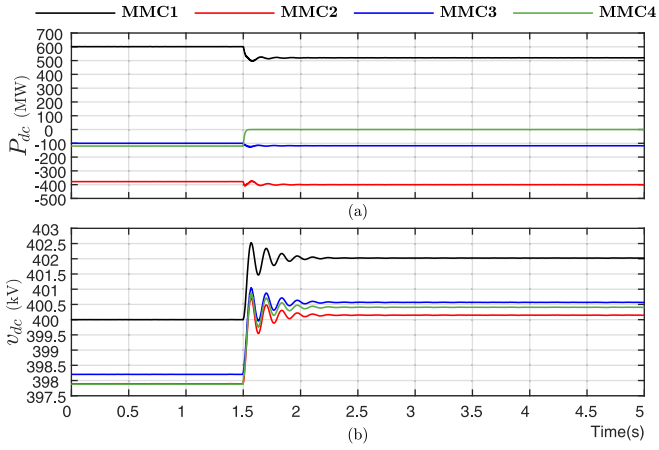

Fig. 9. Waveforms of dc powers and voltages after MMC4 outage under C1: (a) DC power and (b) dc voltage.

Table 8
Power redistribution after converter outage of MMC4 under C1.

Parameter		MMC1	MMC2	MMC3	MMC4
P_{dc} (MW)	Calc.	519.9680	−400.0000	−117.7969	0.0000
	Simu.	520.0655	−400.0000	−117.7626	0.0000
V_{dc} (kV)	Calc.	402.0281	400.1538	400.5749	400.4142
	Simu.	402.0256	400.1499	400.5703	400.4086
K_{droop}		40 MW/kV	0	7.5 MW/kV	0

4.2. Case 2: Power distribution after converter outage under C1

The power redistribution after converter outages of MMC4 with P/V droop control and MMC2 with I/V droop control will be explored in this section. Such study considers converter overloads, while the violation of power limits in all remaining rectifier or inverter stations are not involved.

4.2.1. Case 2.1: Converter outage of MMC4

Following the calculation process in Section 3.3, the power disturbance in MMC4 is 120 MW (ΔP^{PV}_{dc4} = 120 MW) and droop constant is set to zero (K^{PV}_{droop4} = 0) due to MMC4 outage. The derived power in MMC2 exceeds its power rating (|−377.9981 − 38.5549| MW > 400 MW), hence MMC2 runs into constant dc current control and the actual power variation of MMC2 is −22.0019 MW. The derived current variation is −0.0499 kA. The total power variations and voltage deviations are calculated as:

$$\begin{cases} \boldsymbol{\Delta P_{dc}} = [-81.1232, -22.0019, -17.7969, 120.0000]^T \text{ MW}, \\ \boldsymbol{\Delta V_{dc}} = [2.0281, 2.2611, 2.3729, 2.5354]^T \text{ kV}. \end{cases} \tag{33}$$

Fig. 9 shows the waveforms of dc powers and voltages in all four MMCs. The dc power variation and voltage deviation trend after MMC4 outage is similar to the MMC4 reference change, while the converter isolation leads to transient power/voltage oscillations. In addition, the obtained power distributions from calculation and simulation are listed in Table 8.

4.2.2. Case 2.2: Converter outage of MMC2

Since MMC2 adopt I/V droop control in the dc grid, the outage of MMC2 can be expressed as ΔI^{IV*}_{dc2} = 0.95 kA, K^{IV}_{droop2} = 0 and ΔP^{IV}_{dc2} = 377.9981 MW. The derived power variations and voltage deviations are:

$$\begin{cases} \boldsymbol{\Delta P_{dc}} = [-248.2135, 377.9981, -48.6612, -83.9044]^T \text{ MW}, \\ \boldsymbol{\Delta V_{dc}} = [6.2053, 7.4333, 6.4882, 6.7123]^T \text{ kV}, \end{cases} \tag{34}$$

showing that no converter reaches its corresponding power limit, which is the preferred mode of operation. Therefore, MMC1, MMC3 and

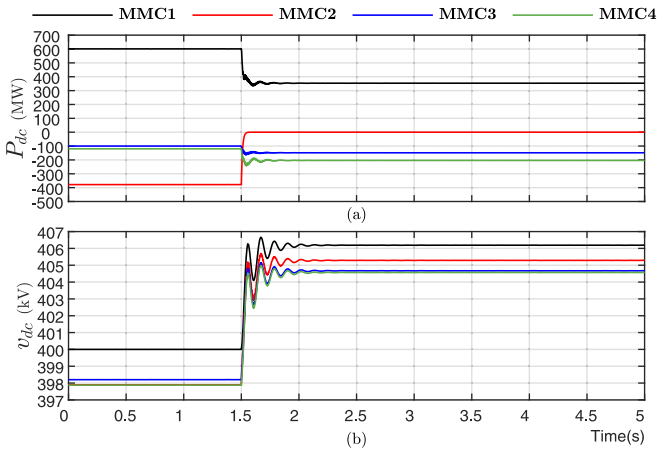

Fig. 10. Waveforms of dc powers and voltages after MMC2 outage under C1: (a) DC power and (b) dc voltage.

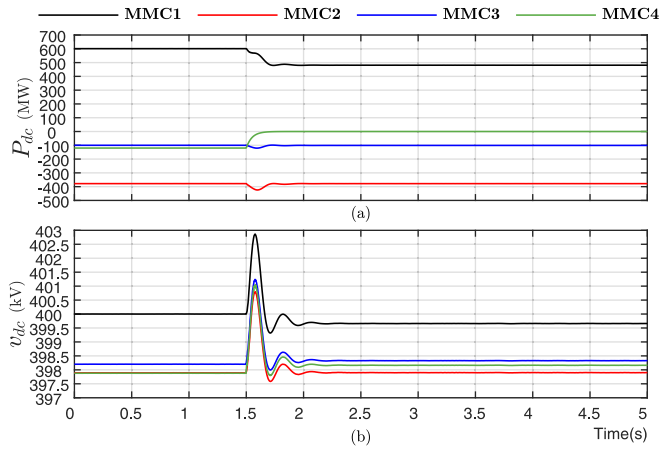

Fig. 11. Waveforms of dc powers and voltages after MMC4 outage under C2: (a) DC power and (b) dc voltage.

Table 9
Power redistribution after converter outage of MMC2 under C1.

Parameter		MMC1	MMC2	MMC3	MMC4
P_{dc} (MW)	Calc.	352.8777	0.0000	−148.6612	−203.9044
	Simu.	353.4931	0.0000	−148.5118	−203.6070
V_{dc} (kV)	Calc.	406.2053	405.3260	404.6902	404.5911
	Simu.	406.1900	405.2885	404.6702	404.5674
K_{droop}		40 MW/kV	0	7.5 MW/kV	12.5 MW/kV

Table 10
Power redistribution after converter outage of MMC4 under C2.

Parameter		MMC1	MMC2	MMC3	MMC4
P_{dc} (MW)	Calc.	481.0912	−378.2691	−100.9980	0.0000
	Simu.	481.0913	−378.1333	−100.9474	0.0000
V_{dc} (kV)	Calc.	399.6667	397.9057	398.3351	398.1700
	Simu.	399.6598	397.8992	398.3283	398.1633
K_{droop}		40 MW/kV	50 A/kV	7.5 MW/kV	0

Table 11
Power redistribution after converter outage of MMC4 under C3.

Parameter		MMC1	MMC2	MMC3	MMC4
P_{dc} (MW)	Calc.	−478.9249	380.4503	100.2725	0.0000
	Simu.	−478.9249	380.5851	100.3265	0.0000
V_{dc} (kV)	Calc.	400.4320	402.1824	401.7523	401.9178
	Simu.	400.4245	402.1754	401.7451	401.9106
K_{droop}		40 MW/kV	50 A/kV	7.5 MW/kV	0

MMC4 maintain the original control schemes, and Fig. 10 shows the dynamic change of dc powers and voltages in all four MMCs. Since the initial dc power of MMC2 is larger than MMC4, the isolation of MMC2 leads to more significant dc voltage deviation (around 1.5%) compared to the case of MMC4 outage. The power distribution calculation results after MMC2 outage are listed in Table 9 which also includes the power distribution simulation results.

4.3. Case 3: Power distribution after converter outage under C2 and C3

The overloads of all remaining converters in the rectifier or inverter side after converter outage are considered in this section by two special control configurations (C2 and C3) in the MMC-based dc grid. The feasibility of proposed excess power reduction strategy is verified for assuring system security after converter outage.

4.3.1. Case 3.1: Converter outage of MMC4 under C2

Different from the converter outage of MMC4 under C1, MMC1 (rectifier terminal) under C2 cannot participate in power coordination with other converters because it adopts constant dc power control. Following the basic power distribution derivation process after converter outage in Section 3.3, the power variation of MMC2 is −87.2852 MW which shows MMC2 is overloaded ($|-377.9981-87.2852|$ MW > 400 MW), hence MMC2 operates with constant dc current control. However, the derived power in MMC3 also exceeds its power rating ($|-100-98.3623|$ MW > 150 MW) when the dc power in MMC2 is −400 MW.

Based on the excess power reduction strategy (26), the reduced power value of MMC1 is equal to the initial power value of MMC4. Hence, the actual dc power variation of MMC1 is −120 MW ($\Delta P_{dc1}^{rec} = \Delta P_{dc1}^{rec*} = -120$ MW). The current power variations and voltage deviations are:

$$\begin{cases} \boldsymbol{\Delta P_{dc}} = [-120.0000, -0.2710, -0.9980, 120.0000]^T \text{ MW}, \\ \boldsymbol{\Delta V_{dc}} = [-0.3333, 0.0130, 0.1331, 0.2912]^T \text{ kV}, \end{cases} \tag{35}$$

which shows no converter is overloaded. Fig. 11 shows the waveforms of dc powers and voltages after MMC4 outage under C2 in simulation.

The power reference of MMC1 (rectifier side) in simulation under C2 is decreased by 120 MW at 1.5 s after the isolation of MMC4. Therefore, the terminal dc voltages are decreased when the system reaches a new steady-state operation. The calculation and simulation results of power distribution are summarized in Table 10.

4.3.2. Case 3.2: Converter outage of MMC4 under C3

MMC1 under C3 functions as an inverter and absorbs power from the other MMCs, hence a new jacobian matrix is obtained as:

$$\boldsymbol{J}_{dc}^{C3} = \begin{bmatrix} 301.5330 & -181.8182 & -121.2121 & 0 \\ -182.7735 & 412.1904 & 0 & -228.4669 \\ -121.7541 & 0 & 487.2654 & -365.2624 \\ 0 & -228.4722 & -365.5555 & 594.3260 \end{bmatrix}, \tag{36}$$

and

$$\boldsymbol{M}_{dc}^{C3} = \begin{bmatrix} -0.2437 & -0.2437 & -0.2441 & -0.2437 \\ 0.1546 & 0.1555 & 0.1532 & 0.1530 \\ 0.0406 & 0.0401 & 0.0427 & 0.0401 \\ 0.0486 & 0.0480 & 0.0481 & 0.0505 \end{bmatrix}. \tag{37}$$

Similar to C2, MMC1 under C3 is also used to maintain constant dc power. The preliminary calculation after MMC4 outage shows MMC2 is overloaded ($|381.9966+85.2399|$ MW > 400 MW), thus MMC2 switches into constant dc current control from I/V droop control. Nevertheless, MMC3 hits power limit as well ($|100+102.0432|$ MW > 150 MW) in the following calculation. Therefore, the total dc power variation in the

Table 12
Comparison between the proposed power distribution derivation method and existing approaches.

Operating scenarios	[9]	[10]	[13]	[15]	[16]	[20,21]	[22]	Proposed method
P/V droop control	✔	✔	✘	✔	✔	✔	✔	✔
I/V droop control	✘	✘	✔	✔	✔	✔	✔	✔
Mixed P/V & I/V droop control	✘	✘	✘	✘	✔	✔	✔	✔
Power disturbance (ΔP^*_{dc})	✔	✔	✘	✘	✘	✘	✘	✔
Current change (ΔI^*_{dc})	✘	✘	✘	✘	✘	✘	✘	✔
Converter outage (P/V droop)	✘	✔	✘	✔	✘	✘	✔	✔
Converter outage (I/V droop)	✘	✘	✔	✔	✘	✘	✘	✔
Converter overloads	✘	✔	✘	✘	✘	✘	✔	✔✔[a]

[a]Overloads of all remaining converters in the rectifier & inverter sides are considered.

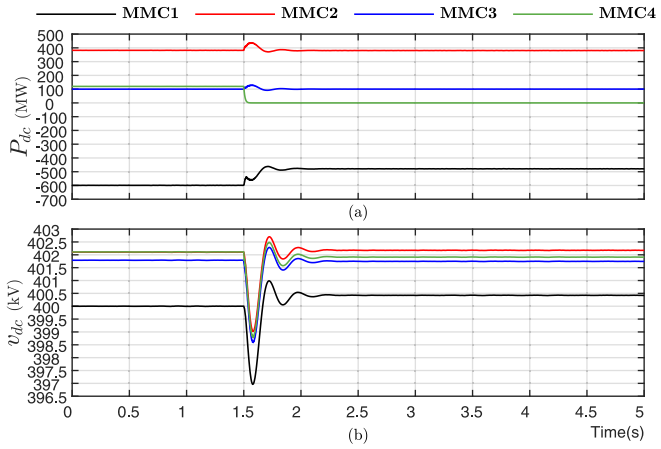

Fig. 12. Waveforms of dc powers and voltages after MMC4 outage under C3: (a) DC power and (b) dc voltage.

inverter side is 120 MW based on the proposed strategy, which reflects in the dc grid is $\Delta P^{inv}_{dc1} = \Delta P^{inv*}_{dc1} = 120$ MW. The new updated power variations and voltage deviations are:

$$\begin{cases} \boldsymbol{\Delta P_{dc}} = [120.0000, -1.5463, 0.2725, -120.0000]^T \text{ MW}, \\ \boldsymbol{\Delta V_{dc}} = [0.4320, 0.0807, -0.0363, -0.1932]^T \text{ kV}. \end{cases} \tag{38}$$

Steady-state and transient waveforms of dc powers and voltages after MMC4 outage are shown in Fig. 12. The rapid power reduction of MMC4 at 1.5 s leads to the transient decrease of grid dc voltage, while the steady-state dc voltage is increased again due to the decrease of dc power reference in MMC1. In addition, Table 11 presents the power distribution calculation and simulation results.

5. Discussion

Section 4 uses an MMC-based four terminal dc grid model with three different control configurations to verify the accuracy of proposed power distribution derivation method under mixed P/V and I/V droop control. The initial operating points for the three control configurations are determined first, then six different operating scenarios are studied in detail. These scenarios include:

1. power distribution after dc power reference change of the MMC with P/V droop control,
2. power distribution after dc current reference change of the MMC with I/V droop control,
3. power distribution after the outage of the MMC with P/V droop control,
4. power distribution after the outage of the MMC with I/V droop control,
5. updated power distribution after all MMC overloads in the inverter side, and
6. updated power distribution after all MMC overloads in the rectifier side.

As the Jacobian matrix (J_{dc}) refers to linear mapping, the obtained calculation results inevitably have minor deviations (<0.01%) compared to the results in simulation. In general, the proposed power distribution derivation for mixed P/V and I/V droop control can be used to (*i*) determine initial operating point, and (*ii*) estimate actual power distribution after power disturbance/current change and converter outages. Table 12 shows detailed comparison between the proposed power distribution derivation method and other approaches in the current literature, and the advantages of the proposed method. The proposed power distribution calculation methodology can be used for the safe power dispatch of an MTDC system or a dc grid, in compliance with $N-1$ safety principles. If used for this purpose, additional RMS or EMT studies would have to be carried out to ensure that the different elements are within their operation limits during the transient.

6. Conclusion

This paper explores steady-state power distributions in MTDC systems and dc grids based on VSCs with mixed P/V and I/V droop control. An estimation-correction algorithm is first proposed to determine the initial operating point, which avoids defining and solve multiple jacobian matrices considering different types of nodes. The power redistributions after outer loop reference changes and converter outages are analyzed in detail. Overloads of converters with P/V and I/V droop control are considered in the power distribution calculation procedure. Moreover, possible overloads of all converter in the rectifier or inverter side after converter outage are studied, and safe post-contingency operation is ensured by excess power reduction strategy. Simulation results of case studies from an MMC-based dc grid with three control configurations verify the accuracy of proposed steady-state power distribution derivation method. Comparisons are also provided to validate the suitability of the proposed method across multiple operating scenarios compared to other methods in the current literature.

Although the proposed derivation approach can accurately estimate the steady-state power redistribution after power/current reference changes and converter outages, it cannot be directly applied in the analysis after converter outage with possible line tripping. Therefore, further work would consider the detailed power distribution considering such line tripping. Moreover, adaptive or deadband droop control can also be considered.

CRediT authorship contribution statement

Pingyang Sun: Methodology, Validation, Investigation, Writing – original draft, Writing – review & editing, Visualization. **Yingqi Wang:** Methodology, Investigation, Writing – original draft, Writing – review & editing. **Muhammad Khalid:** Formal analysis, Writing – original draft, Writing – review & editing. **Ramon Blasco-Gimenez:** Investigation, Writing – original draft, Writing – review & editing. **Georgios Konstantinou:** Investigation, Resources, Writing – original draft, Writing – review & editing, Supervision, Project administration, Funding acquisition.

Declaration of competing interest

The authors declare that they have no known competing financial interests or personal relationships that could have appeared to influence the work reported in this paper.

Data availability

Data will be made available on request.

Acknowledgment

The third author (Muhammad Khalid) would like to acknowledge the support from Deanship of Research Oversight and Coordination (DROC) at King Fahd University of Petroleum and Minerals (KFUPM) through project No. DF201011.

References

[1] N.R. Watson, J.D. Watson, An overview of HVDC technology, Energies 13 (17) (2020).
[2] M.A. Perez, S. Ceballos, G. Konstantinou, J. Pou, R.P. Aguilera, Modular multilevel converters: Recent achievements and challenges, IEEE Open J. Ind. Electron. Soc. 2 (2021) 224–239.
[3] Y. Tian, H.R. Wickramasinghe, P. Sun, Z. Li, J. Pou, G. Konstantinou, Assessment of low-loss configurations for efficiency improvement in hybrid modular multilevel converters, IEEE Access 9 (2021) 158155–158166.
[4] P. Sun, Y. Tian, J. Pou, G. Konstantinou, Beyond the MMC: Extended modular multilevel converter topologies and applications, IEEE Open J. Power Electron. 3 (2022) 317–333.
[5] C. Li, X. Hu, J. Guo, J. Liang, The DC grid reliability and cost evaluation with Zhoushan five-terminal HVDC case study, in: 2015 50th Int. Universities Power Eng. Conf., 2015, pp. 1–6.
[6] H. Pang, X. Wei, Research on key technology and equipment for zhangbei 500 kV DC grid, in: 2018 Int. Power Electron. Conf., 2018, pp. 2343–2351.
[7] X. Wan, Y. Li, M. Peng, Modelling, analysis and virtual parallel resistor damping control of VSC-based DC grid using master-slave control mode, IET Gener. Transm. Distrib. 12 (9) (2018) 2046–2054.
[8] M. Belgacem, M. Khatir, M.A. Djehaf, R. Bouddou, S.A. Zidi, Modeling and control of multi-terminal direct current with voltage margin control strategy, in: 2019 4th Int. Conf. on Power Electron. and their Appl. (ICPEA), 2019, pp. 1–6.
[9] T.M. Haileselassie, K. Uhlen, Impact of DC line voltage drops on power flow of MTDC using droop control, IEEE Trans. Power Syst. 27 (3) (2012) 1441–1449.
[10] L. Xiao, Z. Xu, T. An, Z. Bian, Improved analytical model for the study of steady state performance of droop-controlled VSC-MTDC systems, IEEE Trans. Power Syst. 32 (3) (2017) 2083–2093.
[11] Y. Wang, W. Wen, C. Wang, H. Liu, X. Zhan, X. Xiao, Adaptive voltage droop method of multiterminal VSC-HVDC systems for DC voltage deviation and power sharing, IEEE Trans. Power Deliv. 34 (1) (2019) 169–176.
[12] S. Anand, B.G. Fernandes, Steady state performance analysis for load sharing in DC distributed generation system, in: 2011 10th Int. Conf. on Environment and Elect. Eng., 2011, pp. 1–4.
[13] O. Gomis-Bellmunt, J. Liang, J. Ekanayake, N. Jenkins, Voltage–current characteristics of multiterminal HVDC-VSC for offshore wind farms, Electr. Power Syst. Res. 81 (2) (2011) 440–450.
[14] N.R. Chaudhuri, R. Majumder, B. Chaudhuri, System frequency support through multi-terminal DC (MTDC) grids, IEEE Trans. Power Syst. 28 (1) (2013) 347–356.
[15] J. Beerten, R. Belmans, Analysis of power sharing and voltage deviations in droop-controlled DC grids, IEEE Trans. Power Syst. 28 (4) (2013) 4588–4597.
[16] S. Khan, S. Bhowmick, A comprehensive power-flow model of multi-terminal PWM based VSC-HVDC systems with DC voltage droop control, Int. J. Electr. Power Energy Syst. 102 (2018) 71–83.
[17] W. Wang, M. Barnes, Power flow algorithms for multi-terminal VSC-HVDC with droop control, IEEE Trans. Power Syst. 29 (4) (2014) 1721–1730.
[18] K. Rouzbehi, A. Miranian, J.I. Candela, A. Luna, P. Rodriguez, A generalized voltage droop strategy for control of multiterminal DC grids, IEEE Trans. Ind. Appl. 51 (1) (2015) 607–618.
[19] Y. Zhang, X. Meng, A. Malik, L. Wang, The use of analytical converter loss formula to eliminate DC slack/droop bus iteration in sequential AC-DC power flow algorithm, Int. J. Electr. Power Energy Syst. 137 (2022) 107596.
[20] S. Gao, H. Ye, Y. Du, H. Liu, A general decoupled AC/DC power flow algorithm with VSC-MTDC, in: 2018 13th IEEE Conf. on Ind. Electron. and Appl. (ICIEA), 2018, pp. 1779–1784.
[21] S. Gao, Y. Chen, S. Huang, Y. Xia, Efficient power flow algorithm for AC/MTDC considering complementary constraints of VSC's reactive power and AC node voltage, IEEE Trans. Power Syst. 36 (3) (2021) 2481–2490.
[22] P. Sun, H.R. Wickramasinghe, M. Khalid, G. Konstantinou, AC/DC fault handling and expanded DC power flow expression in hybrid multi-converter DC grids, Int. J. Electr. Power Energy Syst. 141 (2022) 107989.
[23] H.R. Wickramasinghe, P. Sun, G. Konstantinou, Interoperability of modular multilevel and alternate arm converters in hybrid HVDC systems, Energies 14 (5) (2021).
[24] J. Pou, S. Ceballos, G. Konstantinou, V.G. Agelidis, R. Picas, J. Zaragoza, Circulating current injection methods based on instantaneous information for the modular multilevel converter, IEEE Trans. Ind. Electron. 62 (2) (2015) 777–788.
[25] S. Isik, M. Alharbi, S. Bhattacharya, An optimized circulating current control method based on PR and PI controller for MMC applications, IEEE Trans. Ind. Appl. 57 (5) (2021) 5074–5085.
[26] M.S.A. Dahidah, G. Konstantinou, V.G. Agelidis, A review of multilevel selective harmonic elimination PWM: Formulations, solving algorithms, implementation and applications, IEEE Trans. Power Electron. 30 (8) (2015) 4091–4106.
[27] H. Jiang, F. Deng, Z. Wang, Z. Zou, B. Li, F. Blaabjerg, Harmonic optimization strategy for CPS-PWM based MMCs under submodule capacitor voltage reduction control, IEEE Trans. Power Electron. (2021) 1.
[28] H.R. Wickramasinghe, G. Konstantinou, Z. Li, J. Pou, Alternate arm converters-based HVDC model compatible with the CIGRE B4 DC grid test system, 34 (1) (2019) 149–159.
[29] P. Sun, H.R. Wickramasinghe, G. Konstantinou, Hybrid multiterminal HVDC system based on line-commutated and alternate arm converters, IEEE Trans. Power Deliv. 37 (2) (2022) 993–1003.
[30] CIGRE Working Group B4.57, Guide for the development of models for HVDC converters in an HVDC grid, 2014, pp. 129–147.